Appl. Phys. A (2015) 120:1497–1502
DOI 10.1007/s00339-015-9343-5

Applied Physics A
Materials Science & Processing

Hydrogenated nanocrystalline silicon thin films with promising thermoelectric properties

Joana Loureiro[1] · Tiago Mateus[1] · Sergej Filonovich[1] · Marisa Ferreira[1] · Joana Figueira[1] · Alexandra Rodrigues[1] · Brian F. Donovan[2] · Patrick E. Hopkins[2] · Isabel Ferreira[1]

Received: 6 April 2015 / Accepted: 7 July 2015 / Published online: 26 July 2015
© Springer-Verlag Berlin Heidelberg 2015

Abstract The search for materials with suitable thermoelectric properties that are environmentally friendly and abundant led us to investigate p- and n-type hydrogenated nanocrystalline silicon (nc-Si:H) thin films, produced by plasma-enhanced chemical vapor deposition. The Seebeck coefficient and power factor were measured at room temperature showing optimized values of 512 μV K^{-1} and 3.6×10^{-5} W m^{-1} K^{-2}, for p-type, and -188 μV K^{-1} and 2.2×10^{-4} W m^{-1} K^{-2}, for n-type thin films. The thermoelectric output power of one nc-Si:H pair of both n- and p-type materials is $\sim$91 μW per material cm^3, for a thermal gradient of 8 K. The output voltage and current values show a linear dependence with the number of pairs interconnected in series and/or parallel and show good integration performance.

1 Introduction

Thermoelectric (TE) materials have been investigated since the early 1800s, but the doors to the commercialization of TE modules were only opened in the 1950s due to the discovery of Bi_2Te_3 with a figure of merit (ZT) around 1, at near room temperature. Bi_2Te_3 alloys are environmentally unfriendly and rare; therefore, the research on more abundant and green materials must pursue. ZT quantifies the relative efficiency of TE materials and correlates their electrical conductivity (σ), Seebeck coefficient (S) and thermal conductivity (k), for a given temperature (T): $ZT = \sigma S^2T/k$. The total k of a material is defined from both the electron (k_{el}) and phonon contributions (k_{ph}): $k = k_{el} + k_{ph}$. To achieve high ZT values, the power factor ($PF = \sigma S^2$) must be maximized, while k must be minimized. However, all these parameters are interrelated in a way that poses challenging fundamental material science problems to optimize ZT.

Crystalline silicon, one of the most abundant materials on Earth, has a very high S but also high k, posing a serious limitation for its applications in TE devices [1, 2]. Increasing the scattering of phonons (therefore decreasing k_{ph}) is a key factor to decrease k while keeping the mobility of electrons, and k_{el}, high. To fulfill these demands, a number of innovative solutions have been shown such as multilayer configurations, quantum dots and nanocrystalline-structured materials [3–5]. Focusing on these possibilities, we have investigated the thermoelectric properties of nanocrystalline hydrogenated silicon (nc-Si:H) thin films, produced by plasma-enhanced chemical vapor deposition (PECVD). The strong arguments to investigate and improve the TE properties of nc-Si:H include a low temperature, low-cost deposition process, a well-established thin film solar cell industry, material abundance and environment sustainability.

2 Materials and methods

In this work, nc-Si:H films were deposited on corning glass (1 mm thick) using a PECVD system and rf power density between 35 and 90 mW cm^{-3}, substrate temperature (T_s)

✉ Joana Loureiro
joa.loureiro@gmail.com

✉ Isabel Ferreira
imf@fct.unl.pt

[1] CENIMAT/I3N, Departamento de Ciências dos Materiais, Faculdade de Ciências e Tecnologia, FCT, Universidade Nova de Lisboa, 2829-516 Caparica, Portugal

[2] Department of Mechanical and Aerospace Engineering, University of Virginia, Charlottesville, VA 22904, USA

of 150 and 170 °C and total pressure in the range of 1–3 Torr. The gas mixture to produce the p-type and n-type nc-Si:H films consisted of trimethylboron (TMB) and silane (SiH_4), respectively, with a flow ratio (TMB/SiH_4) of 0.26, highly diluted in hydrogen (99 %), and a mixture of silane and phosphine (PH_3) with a flow ratio (PH_3/SiH_4) × 100 of 1.42, with TMB and PH_3 97 % pre-diluted in hydrogen (D_H). These deposition conditions are based on previous studies [6, 7] in order to obtain optimized σ and high crystallinity fraction (X_c). Those studies have demonstrated a remarkable influence of film thickness (up to 80 nm) on the X_c of the bulk and surface layers and also on σ. To ensure crystallinity above 85 %, all samples, in this work, were produced with thicknesses between 100 and 150 nm. Our study focuses on the TE properties variation with the rf power density, for p-type films, and with the change of substrate temperature, for n-type, which are the most significant parameters for each film.

The structural characterization of nc-Si:H films was performed by micro-Raman spectroscopy, spectroscopic ellipsometry (SE), as referred in previous studies [7], and X-ray diffraction (XRD). The relative crystalline fraction, X_{RC}, was estimated via micro-Raman as described by He et al. [8]. Through SE measurements, X_c and X_a (amorphous fraction) were determined by fitting the experimental data of the real and imaginary component of the dielectric function with a multilayer model, as shown in Fig. 1. This model considers the sample stratified in at least two layers (a bulk thick layer and a surface thin layer) both containing a percentage of crystalline and amorphous materials and/or voids material (reference spectra are supplied by Jobin–Yvon software, and it limits the usage of three materials per layer). However, more layers could be added if needed to achieve the lowest error (χ^2) between measured data point and generated data from the model. The model was only considered correct when χ^2 was <1, and only then, the film structure was assumed as well modeled (as in previous work [7]). XRD patterns were collected using a PANalytical X'Pert PRO with Cu$K\alpha$ radiation, at 45 kV and 40 mA, equipped with an X'Celerator detector and performing the scan in a grazing incidence with a step of 0.08° over the angular 2θ range 20°–70°. The analysis of the XRD patterns allows estimation of the crystallite mean sizes and determination of the main growth orientations of the films. The thermal conductivities of the films were measured using time domain thermoreflectance [9–11] (TDTR), an optical pump-probe experiment which utilizes a train of ultra-short laser pulses to induce a modulated heating event on the surface of the sample in the through-plane direction.

The carrier mobility (μ), concentration (N) and electrical conductivity (σ) were obtained in a Bio Rad HL 5500 Hall effect system with a van der Pauw configuration. The activation energy, ΔE, was calculated from the Arrhenius plot of the electrical conductivity as a function of temperature,

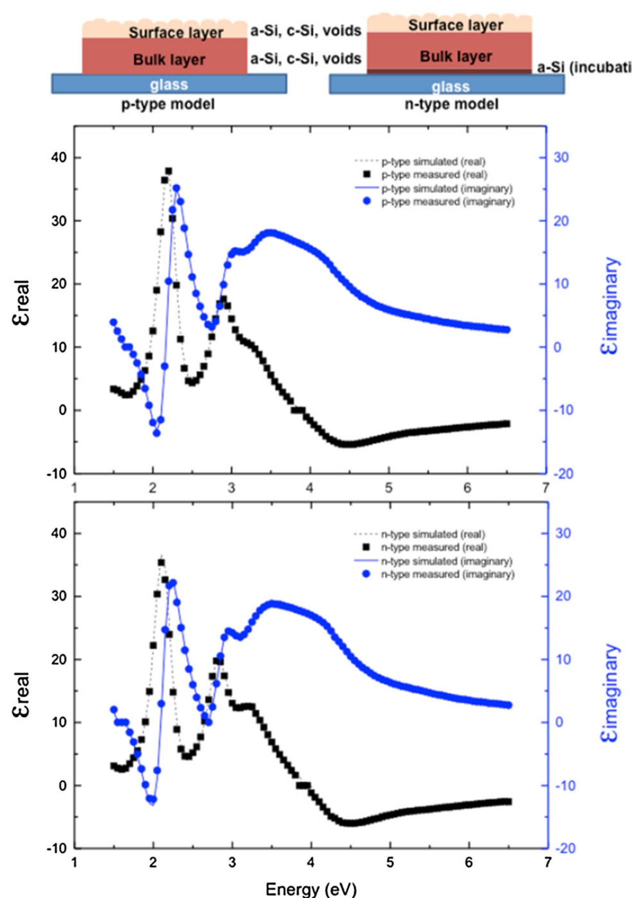

Fig. 1 SE spectra of the real and imaginary component of the dielectric function and corresponding fitted *curve* of the models indicated on the *top* of figure

measured in vacuum and with in-plane contacts, for both n-type and p-type nc-Si:H films. The S coefficient ($S = \Delta V/\Delta T$) was obtained as described in our previous works [12, 13].

TE modules were made by depositing the optimized n-type and p-type nc-Si:H elements on the same glass substrate using a mechanical mask to define the geometry (4 mm wide and 2 mm long) and the interconnection between elements. Two n–p pairs were electrically interconnected in series and then in parallel with other two, in a way that all elements are thermally interconnected in parallel. The maximum output power was obtained from I–V curves acquired using a variable load resistance connected in series with the thermoelectric module, for two temperature gradients (5.5 and 8.5 K).

3 Results and discussion

The crystalline and amorphous fraction of bulk layers (X_{c_b}, X_{a_b}), surface layers (X_{c_s}, X_{a_s}) and the respective layer thickness (d_b and d_s) is shown in Table 1 and is obtained

Table 1 SE results and ΔE of the nc-Si:H films

P (W/cm^3)	d_b/d_s (nm)	X_{c_b}/X_{a_b} (%)	X_{c_s}/X_{a_s} (%)	ΔE (meV)
p-type				
50	98/10	86/7	40/33	56
66	131/9	94/5	45/5	53
75	120/9	89/3	46/25	41
90	124/8	92/2	48/15	35
90[a]	137/7	94/0	62/0	33
n-type				
35	75/9	89/4	53/20	23
69	156/8	93/1	56/20	16
69[b]	105/4	92/0	53/8	17

[a] $D_H = 99.4$; [b] $T_s = 150$ °C

based on the models presented in Fig. 1. Thickness errors are below 1 nm.

Bulk layers with X_c above 85 % and X_a below 7 % confirm high crystallinity for both p-type and n-type films and thickness above 80 nm, as expected. In all samples, X_a and void fraction ($X_v = 100 - X_a - X_c$) of the surface layer are significantly higher than the bulk layers, corresponding to surface roughness. Generically, X_{c_b} and X_{c_s} increase for power density above 50 W cm^{-3}, while X_{a_b} decreases. This behavior substantiates the improvement of p-type films σ from 10.6 to 104 Ωm^{-1} (as shown in Fig. 2a), which is accompanied by a decrease in activation energy from 56 to 35 meV (Table 1). From this, we may conclude that higher power densities have contributed to an increase in incorporation efficiency of the dopant and/or decrease in trapping caused by the amorphous material. In agreement with this conclusion is the observed increase in the carriers' concentration by an order of magnitude, up to 1.2×10^{19} (m^{-3}) and the hall mobility from 0.2 to 0.5 cm^2 V^{-1} s^{-1} (still for p-type films).

With a slight (0.2 %) increase in the D_H used for the deposition of p-type films (due to a slight decrease on the TMB and SiH_4 flow ratio), the X_c was further optimized to 94 % for the bulk layer and 62 % for the surface, while X_a disappeared, leading to the maximum p-type σ value of 138 Ωm^{-1}.

On the other hand, the power density has a minor role on the σ values of n-type films (varying from 3.3×10^3 to 4.6×10^3 Ωm^{-1}) which might be influenced also by their higher thickness and X_c and/or less fraction of voids. These values, consistent with highly dense bulk nc-Si:H materials [7], demonstrate an efficient incorporation of the dopant atoms in the n-type films, which is confirmed by the carrier concentration and mobility values: $N = 3.5 \times 10^{20}$ (m^{-3}) (one order of magnitude higher compared to p-type films) and $\mu_H = 0.52$ cm^2 V^{-1} s^{-1}. The best fitting of SE results also revealed an amorphous incubation layer, thickness

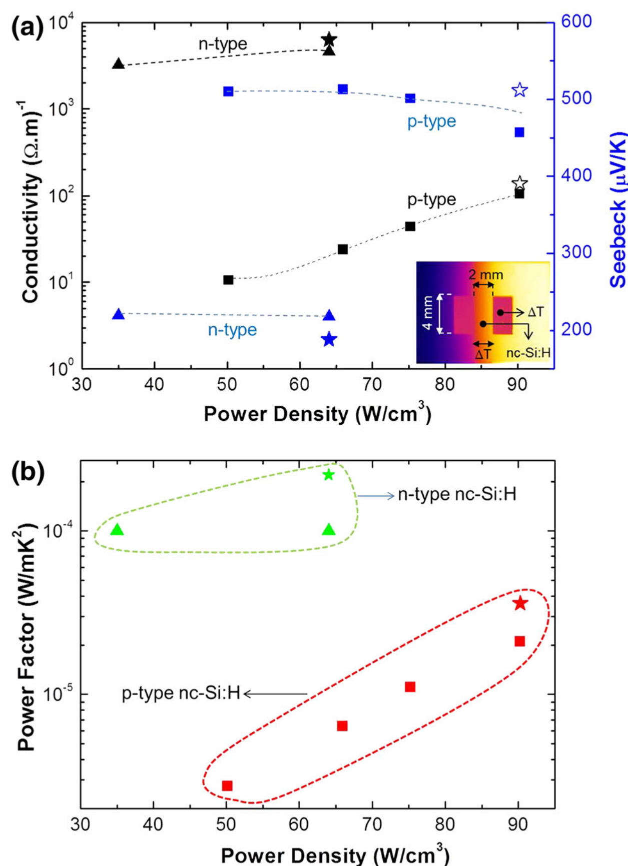

Fig. 2 Influence of power density on σ and S (**a**) and PF (**b**). The *inset* is the thermal image taken with a FLIRA310 thermal camera, showing the ΔT on the sample during the S measurement (dark side—cold; bright side—hot). The inset also shows the shape configuration of the electrodes used. Data are depicted with triangles for n-type films and squares for p-type. The *stars* correspond to the optimized values, having a slight increase in D_H

below 2 nm, present on n-type films, which, in agreement with our previous work [7], was not noticed for p-type films and is not expected to influence the results. The lowering of T_s from 170 to 150 °C, without causing a decrease in crystallinity and keeping high values of $\sigma = 6.4 \times 10^3$ (Ωm)$^{-1}$, $N = 4.8 \times 10^{20}$ (cm^{-3}) and $\mu_H = 0.82$ cm^2 V^{-1} s^{-1}, was successfully achieved only for the n-type films. The only side effect of this variation was a small increase in the surface roughness (X_v increased 15 %) with no further consequences.

The crystallinity was further confirmed by Raman spectra (depicted in Fig. 3a), and small grain sizes were estimated for both types of films from XRD (Fig. 3b). From the micro-Raman spectroscopy, the ratio between the areas of the high-intensity peaks associated with crystalline silicon (c-Si) and nanocrystalline and/or grain boundaries (nc/gb-Si) is 50 and 62 % for n- and p-type films, respectively. As shown in Fig. 3a), the peak related to amorphous silicon (a-Si) is almost absent for both films, in agreement with the SE results.

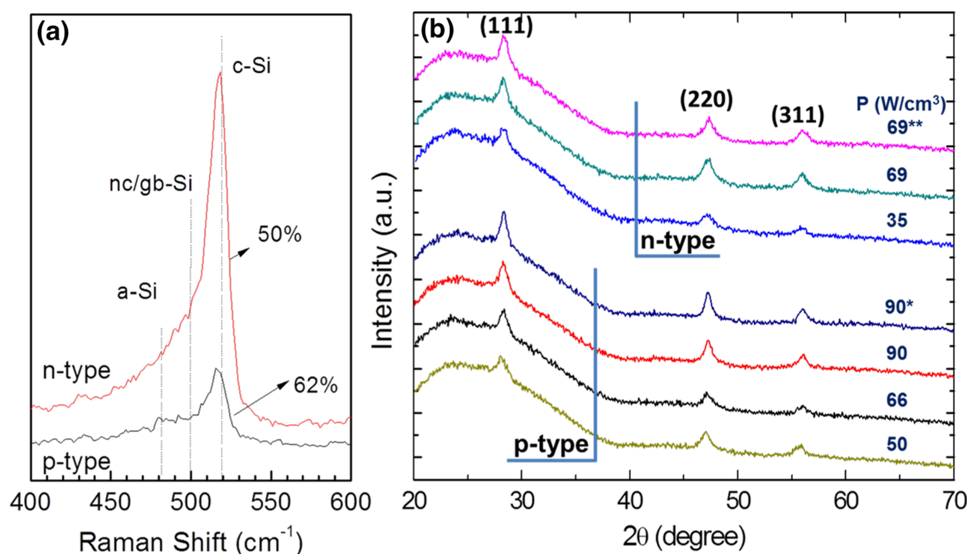

Fig. 3 **a** Micro-Raman spectra of the optimized p- and n-type; **b** XRD spectra of the different films studied. The typical diffraction planes of Si are identified as (111), (220) and (311)

The crystallite mean size obtained from Sherrer equation [14] for the (111) growth direction and corrected from instrumental broadening is 14 nm for n-type with $T_s = 170$ °C and 9 nm for $T_s = 150$ °C. For p-type, a slight increase in mean crystallite size is observed from 14 nm to 18 nm as the power density is augmented. By changing the D_H, the mean crystallite size further increased to 21 nm. Although there is some error associated with size determination, they are clearly less than 25 nm, located in the bulk layer, and do not significantly depend on the studied deposition parameters. That is related to the very high hydrogen dilutions used in the deposition of films that prevents the growth of large grains due to the establishment of equilibrium between deposition of SiH_x and H erosion.

Regarding the thermoelectric properties, it is shown in Fig. 2 that the power density has a minor influence on the S coefficient and remains around 0.5 mV K^{-1} (for p-type films) and −0.2 mV K^{-1} (for n-type films). This finding is contrary to the conventional drop of S when σ increases, but it is consistent with recent observations in heavy boron-doped nanocrystalline Si [15]. The S coefficient is determined by the combined transport in the grain and in the grain boundaries of the nanocrystalline material. Neophytou et al. [15] proposed a concurrent increase in S and σ outcomes from the rise of grain and grain boundaries barrier and/or the width of grain boundary regions. It also claims that it may also be influenced by the precipitation of dopant inside the grains. In order to observe this phenomenon, both nanocrystallinity and extremely high boron doping levels are required. This explanation fits well with our results explaining why S does not show remarkable changes when the power density increases, while for p-type films, σ does. Since the grain size and grain boundaries do not have great variation, as estimated from XRD diffraction, and the doping level in the gas phase is the same, then it is possible that precipitates with the doping elements present in the grains lead to a decrease in activation energy.

The low grain sizes of these materials are expected to contribute to lower the films k, which is fundamental to have high ZT values. The measured k values of the optimized films are 3.3 ± 0.7 W m^{-1} K^{-1} for n-type and 2.7 ± 0.4 W m^{-1} K^{-1} for p-type. In these films, k is limited much more by the grain size than by the film thickness; therefore, the in-plane and cross-plane thermal conductivities will not differ greatly as the phonons in the system will scatter at grain boundaries more readily than from the film boundaries [12, 16, 17]. The uncertainties in these values arise primarily from uncertainty and variation in the thickness of the Al transducer used for TDTR measurements and the nanocrystalline silicon region. These values are in agreement with previous studies showing that nc-Si thin films exhibit much lower thermal conductivities than bulk materials [8, 18–20]. With the above results, the optimized values for power factor and figure of merit, at room temperature, are: PF = 3.6×10^{-5} W m^{-1} K^{-2} and ZT = 4×10^{-3} for p-type and PF = 2.2×10^{-4} W m^{-1} K^{-2} and ZT = 2×10^{-2} for n-type. Although it will be important to improve these values for TE applications, we note that these ZT values of nc-Si:H thin films are above those found in the literature [21, 22] for similar materials. Other authors demonstrated that both p-type and n-type [23] Si nanowires (SiNW) can exhibit PFs one order of magnitude higher than our current nc-Si:H films; however, the production process of our films is simpler and takes profit from an already established technology for very large-area films.

To evaluate the power generation of a nc-Si:H pair (composed of both n-type and p-type elements), the output

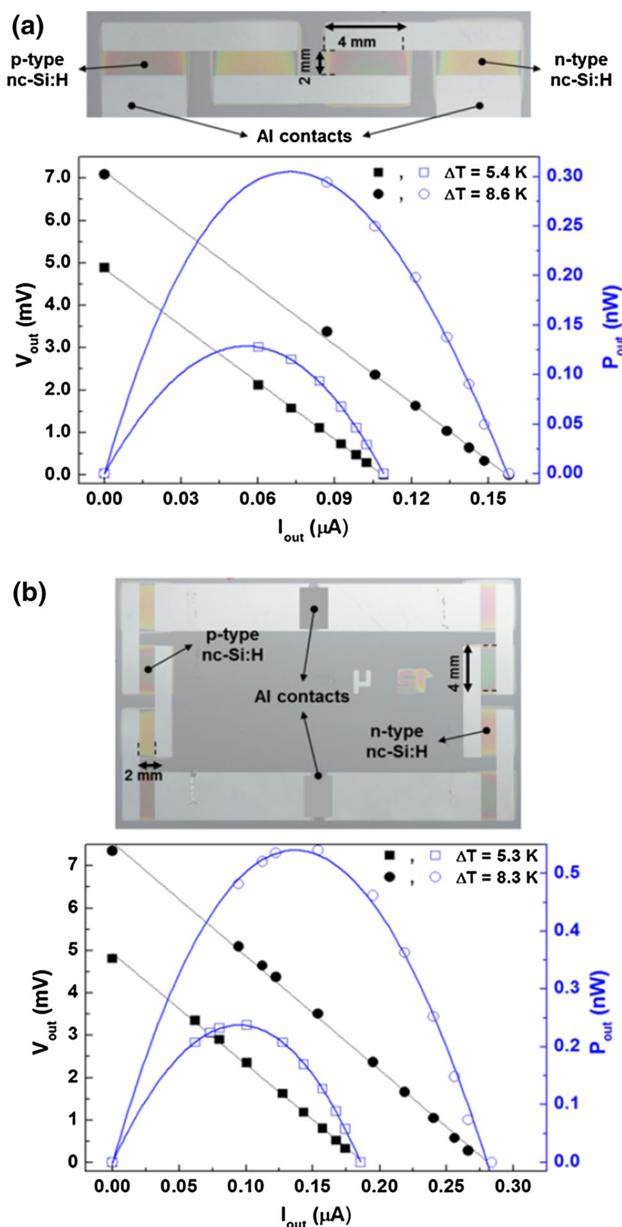

Fig. 4 Output voltage (*solid symbols*) and power (*open symbols*) versus current measured for **a** two pairs and **b** four pairs arranged in two parallel branches, each with two pairs in series, both configurations at a thermal gradient around 5 K (*squares*) and 8 K (*circles*)

voltage and power were measured by changing the load resistance and temperature gradient. As predicted theoretically [13], the current voltage characteristic of a thermoelectric pair is linear, while the output power has a parabolic response with the output current. In order to study the impact of the pair interconnections on the thermoelectric output, two different modules were fabricated: two pairs in series and four pairs (a parallel of two pairs connected in series). The results are shown in Fig. 4a, b. At $\Delta T = 8$ K, the open-circuit voltage, for both modules, is 7 mV, while the output current increases from 0.16 to 0.28 μA with the parallel configuration, leading to a maximum output power of 0.55 nW (almost doubling to output of the series configuration). Hence, the output power is proportional to the number of pairs connected in series and/or parallel meaning that, depending on the application, the TE modules can be designed with the necessary geometry to fulfill the voltage, current and power specifications. The deviations of output voltage and current when associating the modules in series or parallel are due to small variations on the elements resistance related to some shadow effect coming from the masks used to pattern the elements during the deposition, which cause thickness variation. When looking to the maximum output power per volume of TE material (one pair, at $\Delta T = 8$ K), we obtain 91 μW cm^{-3} which enable foreseeing the usage of this technology for heat harvesting in large areas.

4 Conclusions

In summary, p-type and n-type nc-Si:H thin (100 nm) films deposited by PECVD have been presented showing interesting room temperature thermoelectric properties that foreseen their application for large-area energy harvesting. The optimized films, with a crystalline fraction above 92 %, have a PF of 2.2×10^{-4} W m^{-1} K^{-2} for n-type and 3.6×10^{-5} W m^{-1} K^{-2} for p-type while S is -0.19 and 0.5 mV K^{-1}, respectively. Since Si:H is an environmentally friendly and abundant material and TE devices based on it can be fabricated using well-established technology, further investigations to optimize their thermoelectric properties will continue, focusing on post-deposition procedures. With this work, we aim to contribute for a new field of applications for thermoelectric materials, as the thermal losses are the major source of energy losses in actual electrical power sources and large-area harvesting can use less efficient but also less expensive TE materials.

Acknowledgments This work was partially supported by the Portuguese Agency of Innovation (Adi) under project QREN/3435-Nanoxides, by the Portuguese Science and Technology Foundation (FCT), Ministry for Education and Science (MEC), under PEst-C/CTM/LA0025/2011 (Strategic Project—LA 25—2011–2012) and mainly by the NANOTEG project: ENIAC/002/2010. This work was partially supported by the Commonwealth Research Commercialization Fund of Virginia (MF14S-012-En) and Financial Assistance Award No. 01-79-142414, awarded by the US Department of Commerce Economic Development Administration, to the University of Virginia. The content is solely the responsibility of the authors and does not necessarily represent the official views of the US Department of Commerce Economic Development Administration. The material is based upon work partially supported by the Air Force Office of Scientific Research under AFOSR Award No. 5010-UV-AFOSR-0067. The authors would like to thank Márcia Vilarigues from the Conservation Department of FCT/UNL for the micro-Raman measurements and insight.

References

1. W. Fulkerson, J. Moore, R. Williams, R. Graves, D. McElroy, Phys. Rev. **167**, 765 (1968)
2. T. Geballe, G. Hull, Phys. Rev. **98**, 940 (1955)
3. J.-F. Li, W.-S. Liu, L.-D. Zhao, M. Zhou, NPG Asia Mater. **2**, 152 (2010)
4. P. Pichanusakorn, P. Bandaru, Mater. Sci. Eng. R Rep. **67**, 19 (2010)
5. C.J. Vineis, A. Shakouri, A. Majumdar, M.G. Kanatzidis, Adv. Mater. **22**, 3970 (2010)
6. S. Filonovich, H. Aguas, I. Bernacka-Wojcik, C. Gaspar, M. Vilarigues, L. Silva et al., Vacuum **83**, 1253 (2009)
7. S.A. Filonovich, H. Águas, T. Busani, A. Vicente, A. Araújo, D. Gaspar et al., Sci. Technol. Adv. Mater. **13**, 045004 (2012)
8. Y. He, C. Yin, G. Cheng, L. Wang, X. Liu, G. Hu, J. Appl. Phys. **75**, 797 (1994)
9. P.E. Hopkins, J.R. Serrano, L.M. Phinney, S.P. Kearney, T.W. Grasser, C.T. Harris, J. Heat Transf. **132**, 081302 (2010)
10. D.G. Cahill, Rev. Sci. Instrum. **75**, 5119 (2004)
11. A.J. Schmidt, X. Chen, G. Chen, Rev. Sci. Instrum. **79**, 114902 (2008)
12. J. Loureiro, N. Neves, R. Barros, T. Mateus, R. Santos, F. Sergej et al., J. Mater. Chem. A **2**, 6649 (2014)
13. J. Loureiro, R. Santos, A. Nogueira, F. Wyczisk, L. Divay, S. Reparaz et al., J. Mater. Chem. A **2**, 6456 (2014)
14. A. Patterson, Phys. Rev. **56**, 978 (1939)
15. N. Neophytou, X. Zianni, H. Kosina, S. Frabboni, B. Lorenzi, D. Narducci, Nanotechnology **24**, 205402 (2013)
16. B.M. Foley, H.J. Brown-Shaklee, J.C. Duda, R. Cheaito, B.J. Gibbons, D. Medlin et al., Appl. Phys. Lett. **101**, 231908 (2012)
17. B.F. Donovan, B.M. Foley, J.F. Ihlefeld, J.P. Maria, P.E. Hopkins, Appl. Phys. Lett. **105**(8), 082907 (2014)
18. L. Xu, M.P. Garrett, B. Hu, J. Phys. Chem. C **116**, 13020 (2012)
19. T.M. Tritt, D. Weston, in *Thermal Conductivity*, ed. by T.M. Tritt (Springer, US, 2004), pp. 187–203
20. Z. Wang, J.E. Alaniz, W. Jang, J.E. Garay, C. Dames, Nano Lett. **11**, 2206 (2011)
21. R. Lechner, H. Wiggers, A. Ebbers, J. Steiger, M.S. Brandt, M. Stutzmann, Phys. Status Solidi Rapid Res. Lett. **1**, 262 (2007)
22. N. Petermann, N. Stein, G. Schierning, R. Theissmann, B. Stoib, M.S. Brandt et al., J. Phys. D Appl. Phys. **44**, 174034 (2011)
23. Y. Hyun, Y. Park, W. Choi, J. Kim, T. Zyung, M. Jang, Nanotechnology **23**(40), 405707 (2012)